

Review

Utilization of Steel Slag in Road Semi-Rigid Base: A Review

Haibin Li ^{1,2}, Canyang Cui ^{1,2} , Jun Cai ³, Mingming Zhang ^{1,2} and Yanping Sheng ^{4,*}

¹ School of Architecture and Civil Engineering, Xi'an University of Science and Technology, Xi'an 710054, China; lihaibin1212@126.com (H.L.); 20204228114@stu.xust.edu.cn (C.C.); 20204228117@stu.xust.edu.cn (M.Z.)

² Road Engineering Research Center, Xi'an University of Science and Technology, Xi'an 710054, China

³ Qinghai Xihu Expressway Management Co., Ltd., Xining 810001, China; ycc0128@126.com

⁴ School of Materials Science and Engineering, Chang'an University, Xi'an 710064, China

* Correspondence: syp@chd.edu.cn

Abstract: Steel slag (SS) is industrial waste, and there is a large amount of SS to be treated in China. Its disposal generates severe environmental pollution. One of the best ways to use SS is as a road base material. This paper reviews the possibility of using SS in semi-rigid base and evaluates the performance of SS base course. The interaction between three stabilizers (cement, lime-fly ash, and cement-fly ash) and SS is analyzed, and the influence of modifier content on the performance of base course is evaluated. The potential laws between SS, curing time, and unconfined compressive strength, as well as drying shrinkage and temperature shrinkage, are discussed and their effects on the performance of the base course are revealed. The finite element method, discrete element method, and molecular dynamics can be used to analyze the freeze-thaw, rutting resistance, and crack development of SS base. In addition, compared with traditional macadam base, the CO₂ emissions for the use of SS base are slightly more, one of the disadvantages of its use in production, transportation, and compaction. However, considering the overall mechanical, economic, and environmental benefits, it is recommended to use SS in semi-rigid base course. The future research scope of SS as base material is suggested.



Citation: Li, H.; Cui, C.; Cai, J.; Zhang, M.; Sheng, Y. Utilization of Steel Slag in Road Semi-Rigid Base: A Review. *Coatings* **2022**, *12*, 994. <https://doi.org/10.3390/coatings12070994>

Academic Editors: Andrea Nobili and Valeria Vignali

Received: 15 June 2022

Accepted: 6 July 2022

Published: 15 July 2022

Publisher's Note: MDPI stays neutral with regard to jurisdictional claims in published maps and institutional affiliations.



Copyright: © 2022 by the authors. Licensee MDPI, Basel, Switzerland. This article is an open access article distributed under the terms and conditions of the Creative Commons Attribution (CC BY) license (<https://creativecommons.org/licenses/by/4.0/>).

Keywords: steel slag; semi-rigid base; performance evaluation; numerical simulation; environmental impacts

1. Introduction

As an essential symbol of the national industrial development level, steel slag (SS) is one of the most residual solid wastes in the rapid development of its economy and society [1]. In developed countries and regions, SS is widely used in road engineering, concrete aggregate, cement production, fertilizer, and soil modifier [2–5]. The production of SS in China has been ranked first globally since the 21st century. In recent years, the steel output was close to 50% of the world's output [6]. The national steel output was 1.33 billion tons in 2020, and according to the traditional steelmaking method commonly used in China's iron and steel enterprises, the SS produced per ton of iron and steel is approximately 100–150 kg [7,8]. In addition, a total of 133–199 million tons of SS have been produced by 2020. However, less than 30% will be utilized in China. The Chinese Scrap Iron and Steel Application Association has put forward the goal that the total utilization rate of SS will reach 60% in 2025 [9].

Due to its large consumption of aggregate resources, there is a potential market to reuse the solid waste SS as subgrade material in road engineering. With certain technical advantages and market capacity, the road construction industry has gradually becoming the main battlefield of solid waste reuse [10]. However, compared with Japan, Europe, and the United States, the utilization rate of SS in China lags far behind those developed countries (regions). The percentage of SS used in road construction in Japan, Europe, and the United States is 32%, 43%, and 50%, respectively, while only 3% is used in China [11].

The utilization of SS has been studied in developed countries and regions earlier. According to the data from the Japan Nippon Slag Association in 2016, the utilization rate of SS in Japan was as high as 98.4% [11]. Of this, 30.9% of SS was used for soft soil foundation, road subgrade, and embankment [12]. In the United States, the majority of SS was used for road construction, while the remainder was used for marine filler, asphalt concrete aggregate, cement production, and the rest was used for soil pH adjustments and steel reproduction [3]. As the earliest industrialized region in the world, the data of the European SS Association showed that the utilization rate of SS reached 87.0% in 2012 [11]. SS was widely used in geotechnical engineering, road engineering, water conservancy engineering, and railway engineering in Germany early in 2005. In road engineering, Germany used SS for base course and surface course, and tried to mix it with other metallurgical slags as a bearing layer with high bearing capacity [13]. As another industrial power, the UK has widely used SS in the production of cement, highway engineering concrete, and coarse aggregate for road construction [14,15].

Researchers from other developing countries have also carried out research on the utilization of SS in road engineering. Behiry [16] of Egypt mixed SS with limestone aggregate, exploring the influence of SS content on improving the density and strength of base course, and analyzed the relationship between mixture and deflection, stress, strain, and other factors under different content. Kumar and Kumar [17] summarized and analyzed the utilization of SS in India, using SS in road base, and conducted continuous observation after construction, finding that the performance of SS road base was excellent. Karatağ, et al. [18] studied the feasibility of combining SS and macadam in Vietnam for road base, and their results showed that the mechanical properties and porosity were good.

SS is an excellent substitute for natural aggregate [18], which has the advantages of high strength, good wear resistance, durability, and strong stability. It can meet various indexes when used in road base and surface course, and performs better in mechanical properties than natural aggregate [19,20]. Compared to natural aggregate, SS has more apparent edges and corners, a rougher surface texture, and better wear resistance [21]. At the same time, the micropores on the surface of SS are conducive to combining with cement and improving its strength [22], showing its potential utilization in road base.

As the bearing layer of the road, the road base can be divided into rigid base, semi-rigid base, and flexible base according to the different mechanical characteristics. Since the 1970s, semi-rigid base has been rapidly promoted in China because of high bearing capacity, high stiffness, comprehensive material sources, and low cost. Recently, semi-rigid stabilized base asphalt pavement has become one of the typical structures of high-grade roads in China [23]. Various types of the semi-rigid bases have received extensive attention [24], such as cement stabilized base [25,26], lime stabilized base [27], lime-fly ash stabilized base [28,29], and cement-fly ash stabilized base [30]. However, the aggregate utilization of semi-rigid base is extensive, which has a significant impact on the ecological environment. With the continuous attention to global sustainable development and cleaner production [31], how to reduce environmental pollution and save resources has also becoming a critical research direction of road researchers. In recent years, researchers have increased the use of industrial by-products [32–35] in road base, such as SS, fly ash, coal gangue, etc. Alternatively, waste base materials are recycled [36,37].

However, little research has been done on the utilization of SS as semi-rigid road base material. The paper aims to review and highlight the possibility of using SS as semi-rigid base material, evaluating the performance of SS base and its impact on the environment. The flowchart of the review is shown in Figure 1.

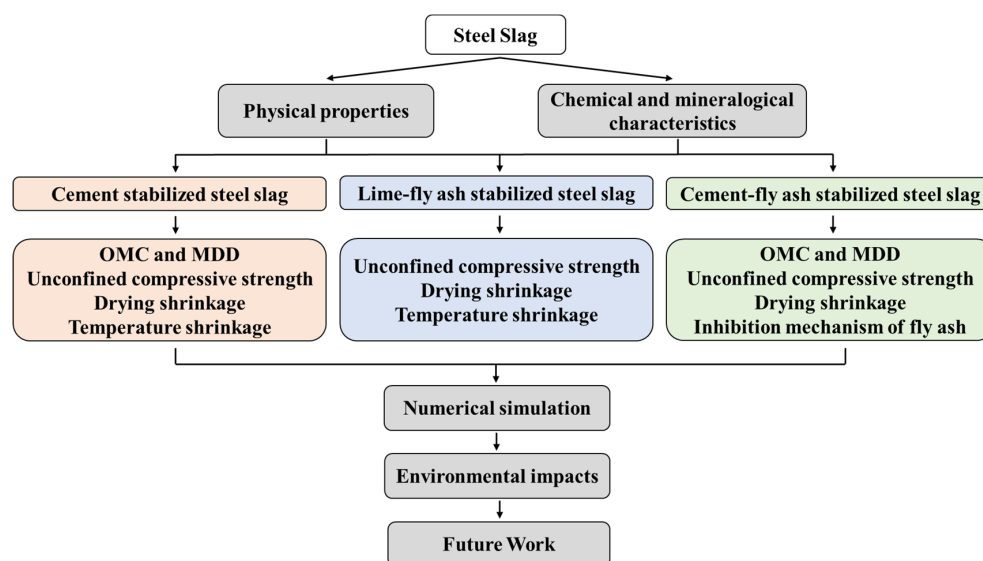


Figure 1. Flowchart of the review.

2. Materials

2.1. Physical Characteristics of SS

The physical and mechanical properties of SS from the present paper are shown in Table 1. In most of the relevant literature, the apparent specific gravity of SS is shown to be higher than 3.20 g/cm³. The crushing value of the aggregate is used to measure the crushing resistance of the aggregate under increasing load. It is a vital index to measure the mechanical properties of the stone to evaluate its applicability in road engineering. The crushing value of SS ranges within 10%–21%, and all meet the requirements of less than 22% in the standard [24]. SS has a porous surface, with more open pores and higher water absorption than ordinary macadam. Elongated and flaky particles (EFP) will form large pores, greatly weakening the intercalation of aggregates and affecting the road performance of the mixture. According to Table 1, the EFP content of SS is very low, almost all particle sizes are less than 10%.

Table 1. Physical properties of SS from the researched literature.

Particle Size (mm)	ASG (g/cm ³)	CV (%)	LA (%)	WA (%)	EFP (%)	References
4.75–9.5	-	10.3	8.5	-	10.1	[38]
≥9.5	-				6.7	
0–4.75	3.37	23.5	-	1.33	0.0	[39]
4.75–16	3.48					
16–26.5	3.47					
0.06–50	3.34	-	20	0.85	-	[16]
0.075–31.5	3.31	16.7	21.5	0.43	5.7	[40]
<1	3.35	-	-	0.40	-	[41]
0.075–31.5	3.50	16.3	12.05	2.00	1.1	[42]
0–25	2.90–3.20	-	-	≤1.50	-	[43]
5–10	3.25	13.6	13.2	2.70	5.1	[44]
10–16	3.26			1.96	(4.75–9.5mm) 4.3 (>9.5mm)	
0.075–31.5	3.24–3.36	17.5	18.5	0.46	4.6	[45]
0.075–31.5	3.55	14.5	11.8	2.60	4.7	[46]
0–5	-	-	-	-	-	[47]
0–25	-	19.7	-	-	-	[48]
0.075–31.5	-	20.7	-	-	-	[49]
0–10	3.14	-	-	4.44	-	[50]

2.2. Chemical and Mineralogical Characteristics of SS

Generally, SS can be categorized into four types based on the production process: blast furnace slag, basic-oxygen furnace slag, electric-arc furnace slag, and ladle furnace slag [51]. However, in the selection of semi-rigid base materials, little information about the types of SS is mentioned in the previously referenced published paper. It means that SS used for semi-rigid base is not usually considered with regards to production process, but rather regarding its basic performance. The chemical composition of SS from the previous studies is shown in Table 2. SS has a higher density than limestone and granite because of its high iron content [52]. The relative proportion of Al_2O_3 and SiO_2 is high, and tricalcium silicate and active mineral calcium aluminate are formed in the later stage. When SS contains a greater proportion of CaO, then it has a greater alkalinity and has a greater activity [53]. CaO can react with SS and water, and the pH can reach 10–12, which has a certain anti-corrosion effect [40]. Free calcium oxide (f-CaO) is generally considered to be the main problem in terms of swelling in water [54,55]. The content of f-CaO in the researched literature is lower than the recommended limit [56].

Table 2. Chemical composition of SS from the researched literature.

CaO	$\text{Fe}_2\text{O}_3+\text{FeO}$	SiO_2	MgO	MnO	P_2O_5	Al_2O_3	SO_3	$\text{Na}_2\text{O}+\text{K}_2\text{O}$	f-CaO	References
51.23	16.78	8.59	3.93	2.26	1.52	1.29	0.30	-	2.47	[39]
-	89.00	1.00	-	-	-	-	-	-	-	[16]
66.58	3.20	21.86	1.39	-	-	5.46	0.32	0.91	-	[46]
52.52	0.33	23.72	4.50	0.97	-	2.26	0.76	-	-	[47]
40–50	7–10	10–15	10.82	-	3–5	-	-	-	2.10	[48]
21.08	12.84	14.21	13.49	-	-	5.83	-	-	-	[49]
24.98	25.45	17.08	10.58	8.91	-	5.40	0.25	0.25	-	[57]
45.90	11.20	16.30	6.50	-	4.10	9.70	-	-	-	[58]
42.72	25.02	15.77	4.79	4.79	0.86	6.07	-	0.08	0.71	[50]
19.59	40.74	22.69	0.23	0.13	0.60	12.75	-	-	<0.01	[59]
35.30	1.20	33.40	6.50	0.75	-	18.20	-	-	-	[34]

3. Performance Evaluation and of SS Mixtures

3.1. Cement Stabilized Steel Slag (CSS)

The volume expansion of SS can be reduced by natural weathering, aging, or chemical treatment [11,60,61]. Table 3 shows that part of SS is aged or pretreated before being used for base course to reduce volume expansion. The combination of SS and macadam cannot only be applied for the full utilization of the active components of SS and avoid overstrength, but also for good stability [49]. Through the mechanical test, it is found that adding SS can improve the mechanical properties of the mixture, which is better than the traditional semi-rigid base [13]. It is possible to improve the performance of the base course using SS, but consuming a great deal of SS and improving resource utilization can also be achieved by using SS as a partial or complete replacement for macadam. However, the research on CSS started late and there are few relevant engineering and technical standards.

3.1.1. OMC and MDD of CSS

There are many factors affecting OMC and MDD determined by the compaction test, especially the influence of compaction work and the particle size gradation of SS. The compaction work is defined, and the transmission of compaction work and the movement effect among SS particles in different gradations are different, so the OMC and MDD under different SS gradations are different. MDD and OMC play an important role in the compaction, which many mechanical property tests are based on. Therefore, it is essential to study OMC and MDD of CSS.

Table 3. Components and properties of CSS from the researched literature.

Treatment	SS: Macadam Content (%)	Cement Content (%)	OMC (%)	MDD (g/cm ³)	References
-	69:31	5	4.60	-	[38]
-	30:70, 50:50, 70:30	3.5/4/4.5	4.72–5.14	2.39–2.56	[39]
-	100:0	3/4/5	6.72–8.52	2.72–2.75	[40]
Pretreat	100:0, 90:10, 70:30, 50:50, 0:100	4/5/6	4.90–5.85	2.31–2.38	[41]
Aged 1 year, Pretreat (fly ash)	75:25, 50:50, 25:75, 0:100	-	4.71–5.37	2.49–2.74	[42]
-	100:0, 60:40	5	4.70–5.60	2.65–2.66	[44]
-	100:0	3/4/5	6.73–8.51	2.71–2.75	[45]
Aged	85:15, 65:35, 55:45, 0:100	4/5/6	3.80–5.30	2.23–2.68	[46]
Pretreat (NaOH)	100:0	5/8/10/14	-	-	[47]
Aged 6 months	100:0	1/2/3/4/5	7.70–8.30	2.62–2.64	[48]
Aged	75:25, 50:50, 25:75	3	5.50–7.00	2.25–2.41	[49]
-	100:0, 75:25, 50:50, 25:75, 0:100	2/4/6	-	2.26–2.53 (7d) 2.28–2.60 (28d)	[57]
-	100:0, 75:25, 50:50, 25:75, 0:100	3	4.30–7.00	2.27–2.63	[58]

Figure 2 shows that the law of OMC and MDD of CSS with different proportions is significant. The higher the SS content, the greater OMC of the mixture and MDD. It can be explained that the water absorption of SS is smaller than that of crushed stone, which is also consistent with the physical characteristics of the SS in Section 2.1. The OMC and MDD of 0% SS mixture are significantly less than 100% SS.

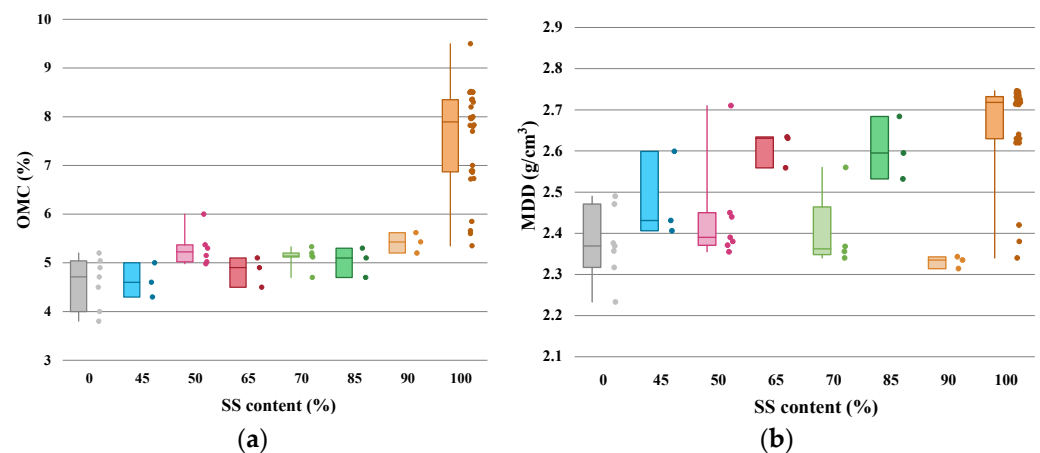


Figure 2. The relationship between (a) OMC, (b) MDD and different SS content (Adapted from [39–42,44–46,48,49,58]).

The difference of SS gradation will cause the change of its OMC and MDD, as shown in Figure 3a. The particle size ranges of SS for coarse, fine and intermediate are 0.075–31.5 mm [40,49]. According to the specification of China, the upper, middle, and lower limits of the gradation range are selected as three kinds of gradations [40]. The finer the SS gradation, the greater OMC and the smaller MDD, but the change range of MDD is small. It can be explained that the finer gradation contains more fine materials and has a more prominent specific surface area. The fine SS particles have high water absorption, so the water content of the mixture will become larger. The coarser gradation contains more coarse materials, and the skeleton structure formed between the coarse materials makes MDD larger than that of the finer gradation. However, the fine gradation is more likely to develop a dense structure due to the large amount of fine materials, so MDD is similar.

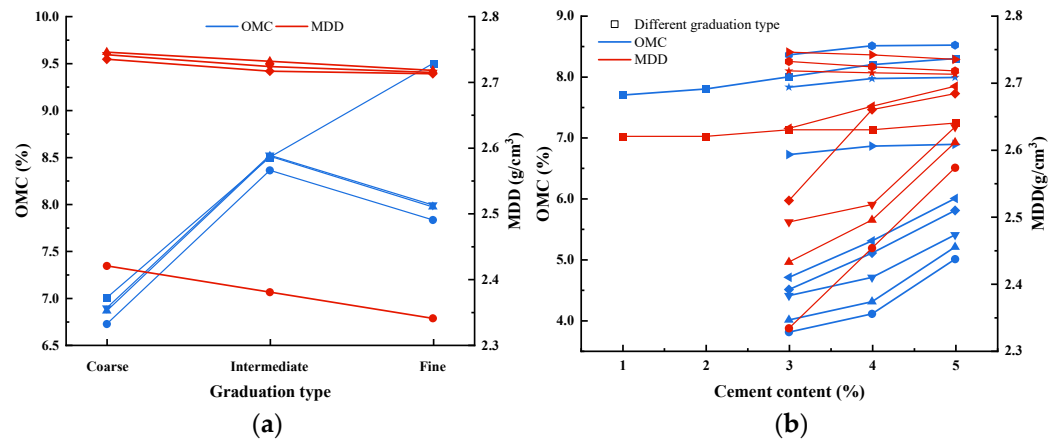


Figure 3. (a) The relationship between OMC, MDD and grading particle size of SS (Adapted from [40,49]) (b) OMC, MDD of different SS contents (Adapted from [40,48,62]).

Figure 3b shows that OMC increases with the addition of cement content. However, due to different materials and gradation types, the growth range of OMC is 0.4%–31.6%, when the cement content increases from 3% to 5%. The MDD shows a similar trend with the OMC. The increasing rate of most MDD ranges from 1.9% to 10.3%. MDD values dropped slightly in two sets, but fluctuated within 0.5%. Due to the difference of materials, it is considered negligible.

3.1.2. UCS of CSS

With the increase of SS, UCS increases continuously, as shown in Figure 4a. UCS of 7d meets the requirements of medium and light traffic of high-grade roads in China. When the content of cement exceeds 5% and SS exceeds 40%, it meets the requirements of heavy traffic (4 MPa) [63].

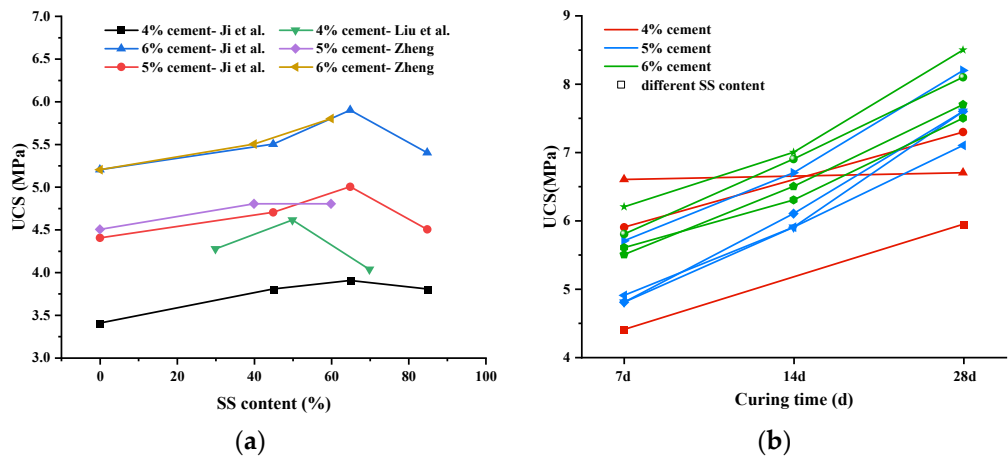


Figure 4. (a) UCS of different SS and cement contents (Adapted from [39,46,62]) (b) UCS of different curing time (Adapted from [39,46,62]).

Some studies show that UCS increases with the SS content increasing [49,62,64]. The addition of crushed stone directly reduces SS, and the reduction of active components in SS will inevitably have a negative impact on the compressive strength. When the crushed stone exceeds 75%, its compressive strength is almost the same as 100% crushed stone [49]. The reason is that a small amount of SS does not play a decisive role in the strength, and only when the amount of SS accounts for a large proportion will the 7d compressive strength be greatly improved.

Other researchers have found an optimal SS content between 40% and 80%, within which the UCS value can reach the maximum [39,42,46]. When the SS content increases

from zero to the optimal content, the damage resistance is effectively improved. This is because the high strength and rough surface structure of SS cause the UCS to increase continuously. In addition, C_3S and C_2S cementitious components in SS form C-S-H gel to make the system stronger [65]. When the SS content is further increased, CSS will produce more harmful pores [66]. CSS has high porosity and water absorption, leading to a large internal gap of the sample, which is not conducive to the formation of strength.

When the cement content is low, the 7d UCS of CSS is low. It can be explained by the fact that there are many pores on the surface of SS, and some cement particles gather on the surface of SS so that this part of the cement cannot be hydrated quickly. In the case of low cement content, the adsorption of SS reduces the amount of reactive cement, which is not conducive to improving the compressive strength of the mixture.

With the same cement content and SS content, the UCS of CSS rises with the curing time increasing, as shown in Figure 4b. The appearance of SS can be seen clearly as shown in Figure 5a. It can be seen that there is a small amount of white floccules on the outer surface of SS, which is C-S-H gel. The number of products in the field of vision is not dense, indicating that SS has just begun to react with water. In the first 7 days of curing, the reaction inside CSS is relatively slow, and there are not many substances generated. Meanwhile, there are many pores on the surface of SS, and some cement particles gather on the surface of SS which cannot be hydrated quickly [62]. The adsorption of SS reduces the amount of reactive cement, which is not conducive to improving the compressive strength of the mixture. Therefore, the compressive strength of the mixture cannot be significantly improved at the initial stage. After 28 days, the white floccules have basically wrapped the SS, and the original appearance of the SS can hardly be seen, as shown in Figure 5b. The strength of CSS is mainly provided by skeleton strength, hydration, and pozzolanic reaction of SS. There are similar active ingredients in cement and SS, which will hydrate calcium silicate, hydrated calcium aluminate, hydrated calcium ferrite, and calcium hydroxide after reacting with water. The active silicon dioxide and aluminum oxide components in SS can react with calcium hydroxide to produce hydrated calcium silicate and hydrated calcium aluminate. As the curing time increases, a large number of substances are generated in CSS, which are closely connected to the SS and crushed stone particles to form a firm structure and improve the overall strength of the mixture.

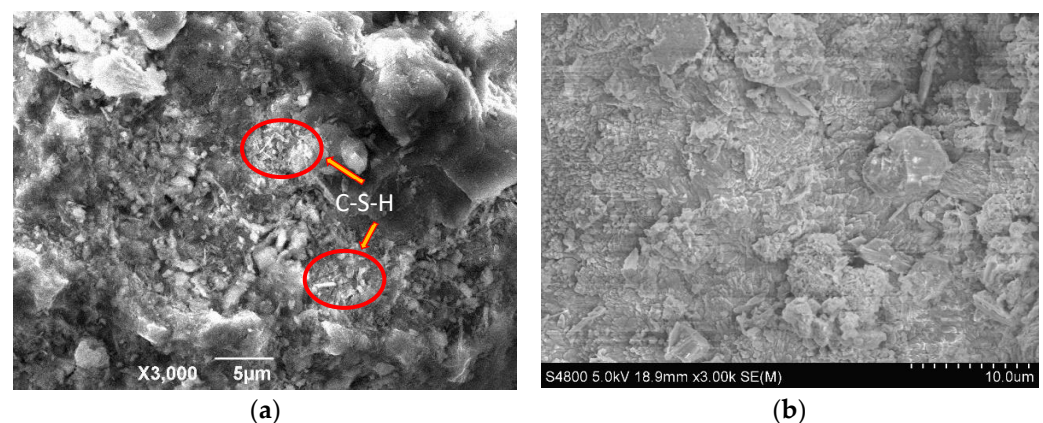


Figure 5. (a) After 7d; (b) After 28d; SEM images of CSS ($\times 3000$ times) (Adapted from [62]).

With the increase of cement, the UCS of CSS also increases. The cement is continuously hydrated in the mixture, and the compressive strength of the mixture increases. There are few reaction products at first. The SS activity in the mixture is low, and the reaction speed is slow. However, with the increase of curing time, the activity of SS is slowly stimulated, the reaction is constantly accelerated, and the cementitious products are also continuously increased, increasing the compressive strength of the mixture [67,68]. Despite reducing cement hydration rates in the early stages, SS can boost cement hydration later. In addition, SS will

also react with water to increase the compressive strength of the mixture. Therefore, at the same cement content, the more macadam replaced by SS, the greater the UCS of the mixture.

3.1.3. DS of CSS

The cement stabilized base course is easy to crack under long-term load or when the ambient temperature changes. After the cracking of the base course, the integrity of the base course can be destroyed with the cracking of the pavement surface. The relationship among water loss rate, DSC, and time is shown in Figure 6. The water loss rate and DSC of different mixing ratios show similar growth trends, and they are close to the level with the increase over time [39–41,62,64]. The water loss rate of the CSS mixture is greater than that of the CSM mixture, indicating that the water absorption performance of SS is better than that of macadam, and the hydration effect of CSS is more evident than that of CSM [40]. Therefore, when SS is used as base material, special attention should be paid to field construction in the first two weeks to avoid adverse impact of water loss on the performance of base [39,58]. The high-water loss rate in the early stage occurs when the specimen is saturated, the cement and SS in the mixture react with water to consume water, and a large amount of free water will evaporate from the specimen. The greater the internal reaction of the mixture in the early stage, the greater the water loss, making the water loss rate in the early stage more prominent. After that, the specimen will consume more water in the early stage, and the products generated by hydration reaction are wrapped on the surface of cement and SS particles. Therefore, the hydration reaction rate of cement and SS is slowed down and the water consumption is reduced. Thus, the water loss rate will gradually decrease in the later stage.

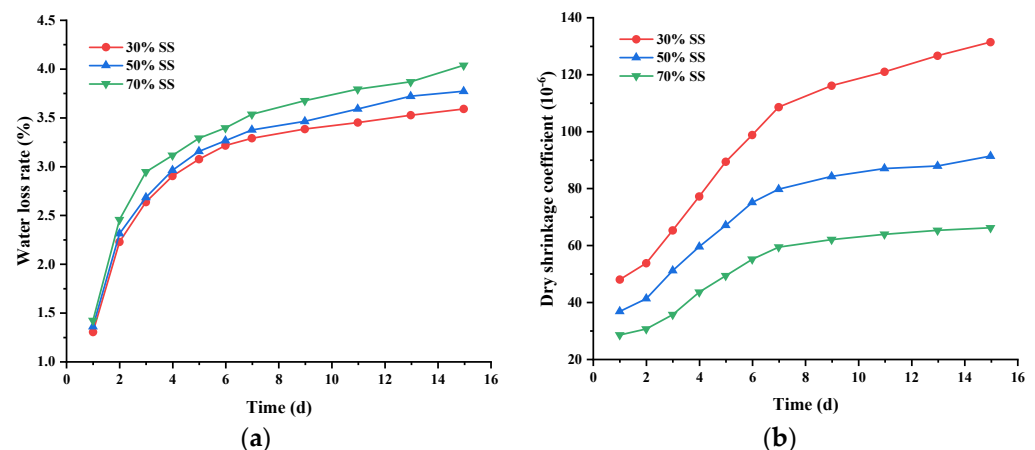


Figure 6. (a) The water loss rate of CSS with curing time (Adapted from [39]). (b) Dry shrinkage development of CSS with different SS contents (Adapted from [39]).

At the same cement content, the greater the amount of SS, the greater the water loss rate of the mixture and the smaller the DSC [39–41,62,64]. The DS of materials is caused by the shrinkage of pores caused by water evaporation, resulting in the change in overall macro volume. The micro expansion of active components such as f-CaO in SS in contact with water makes up for this defect, thus reducing the DS of the material [39,40,62,64,69]. Therefore, CSS as pavement base or subbase material can effectively slow down the formation of pavement reflection cracks. According to the research of Xu [70], DSC becomes 42% less with 50% SS added after 90 days of curing.

Under the same SS content, the more the cement content, the greater the water loss rate of the mixture, and the DSC increases to a certain extent, but it is not significant [62,70]. Based on 40% and 60% SS content, Zheng [62] increased the cement content by 1%, resulting in the DSC increasing by 7.1% and 9.7%, respectively. Similarly, the cement content was increased by 1%–2%, which caused a 10% increase in the DSC of the specimens with four SS contents [70].

3.1.4. TS of CSS

The average value of TSC corresponding to each temperature interval in the TS test results represents the overall level of shrinkage performance of SS mixtures related to temperature change, as shown in Figure 7. The development law of TSC is opposite to that of DSC. The increase of temperature causes the expansion of water, and the expansion pressure of water increases the particle spacing, resulting in the expansion of base materials [40]. With the same cement content, the TSC of CSS mixture increases with the increase of the content of SS. Due to the SS reaction with water, the hydration products and secondary minerals in CSS mixture will increase. Compared with macadam, it is more sensitive to the change in temperature [39,40,62]. The research results of Zheng [62] are shown as follows: under the content of 5% cement, the average TSC of CSM was $7.5 \times 10^{-6}/^{\circ}\text{C}$. When the content of SS was 40% and 60%, the TSC of CSS increased by 14.7% and 25.3%, respectively. Similarly, under the content of 6% cement, the average TSC of CSM was $8.7 \times 10^{-6}/^{\circ}\text{C}$. When the content of SS is 40% and 60%, the TSC of CSS increased by 19.5% and 29.9%, respectively. The cement content will affect the TS deformation of base material [40,62]. In the case of the same SS content, adding 1% cement would increase the TSC by 20.9% and 20.2%, respectively.

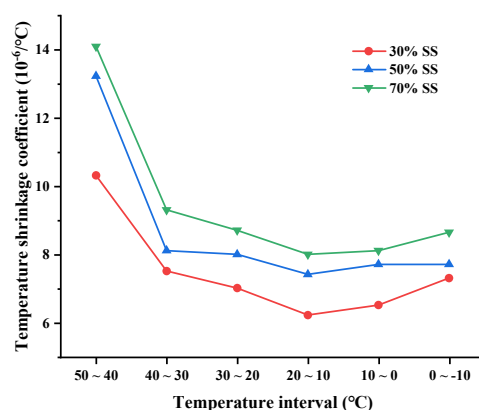


Figure 7. Temperature shrinkage of CSS with different SS contents (Adapted from [39]).

The cracking of CSM base is mainly caused by DS. It can be seen from the comparison between Figures 6b and 7 that the DS of CSS base is much greater than the TS. Although the TSC of the mixture increases with adding SS into CSM, the increased value is far less than the decrease of DSC. Therefore, due to the addition of SS into CSM, the DS of base course is greatly reduced, which indicates that the crack resistance of base course is enhanced. Furthermore, SS added to CSM improves the strength of the base course as well. In conclusion, on the premise of meeting the strength design requirements of the base course, the amount of cement in CSS mixture can be appropriately reduced, and the strength still meets the requirements. By reducing cement content, the economic cost of CSS will be reduced, and the DS and TS of the base will also be reduced so that crack resistance will be improved.

3.2. Lime–Fly Ash Stabilized Steel Slag (LFSS)

Fly ash is another type of industrial waste. The combination of fly ash and SS can not only obtain better environmental benefits but also inhibit the expansion of SS. The use of fly ash as a stabilizer for SS base has been widely studied, as in LFSS [59], lime–fly ash stabilized steel slag and crushed stone [71], fly ash–steel slag soil [72], and fly ash–steel slag–phosphogypsum [73]. Due to a relative scarcity of studies on other types, this paper mainly focuses on LFSS with 100% SS as aggregate. The traditional lime–fly ash soil base shows low early strength, and the addition of SS can effectively improve the early strength of the base for the characteristics of SS. Components and properties of LFSS from the researched literature are shown in Table 4.

Table 4. Components and properties of LFSS from the researched literature.

Lime: Fly Ash Content (%)	Binder: Aggregate Content (%)	OMC (%)	MDD (g/cm ³)	References
1:3	16:84	5.60–6.10	2.29–2.58	[58]
1:3	1:2.5, 1:3, 1:3.5, 1:4	8.10–10.60	2.07–2.28	[59]
6:19, 1:3, 4:11	25:75, 20:80, 15:85	8.7–14.0	1.69–2.00	[74]
1:3	25:75, 20:80, 15:85	-	-	[75]

3.2.1. UCS of LFSS

When the lime-to-fly ash ratio is 1:3, the UCS relationship of LFSS of various mix proportions is shown in Figure 8. It can be seen that the 7d UCS exceeds 4 MPa, which is much higher than the requirements for the extra heavy traffic on expressways in the specification (1.1 MPa) [63]. In LFSS mixture, SS is used as the skeleton to provide strength and stiffness for the mixture. Lime and fly ash as fillers must also maintain a certain proportion to ensure the long-term strength and durability of the LFSS mixture. The increase of the mixture's compressive strength mainly depends on the pozzolanic reaction of lime and fly ash [59]. With the increase of aggregate proportion, UCS values continue to improve. Pai, et al. [59] found that when the binder-to-aggregate ratio increased from 1:4 to 1:2.5, the UCS decreased by 20% (7d) and 19% (14d), respectively. Because the pozzolanic reaction is slow, the increase of curing time can significantly improve UCS value [59]. When the binder-to-aggregate ratio is 1:3, the UCS of 14d and 28d was 64% and 83% higher than that of 7d. When the binder-to-aggregate ratio is 1:4, the UCS value of 14d and 28d was 33% and 64% higher than that of 7d.

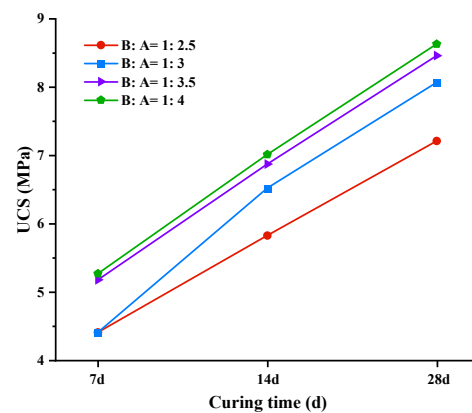


Figure 8. UCS of different curing time (lime-to-fly ash ratio = 1:3, B: A denotes binder-to-aggregate ratio) (Adapted from [59]).

As shown in Figure 9a, when the ratio of lime-to-fly ash is approximately 1:3, the 7d compressive strength of the binder is the largest. The addition of little lime cannot fully stimulate the activity of fly ash, resulting in a slow reaction of pozzolanic ash and low early strength. The influence of the lime-to-fly ash ratio on the compressive strength of the mixture can be seen from Figure 9b. The compressive strength of all proportions of the LFSS mixture is higher than 1.1 MPa, meeting the specification requirements [63]. Although the ratio of lime-to-fly ash can be from 1:2 to 1:5, due to quality and economic reasons, the ratio of 1:3 is more adopted, which is consistent with the data of Table 4. When the lime-to-fly ash ratio is between 5:15 and 4:16, the compressive strength result of LFSS mixture is better, which further explains the rationality of the lime-to-fly ash ratio.

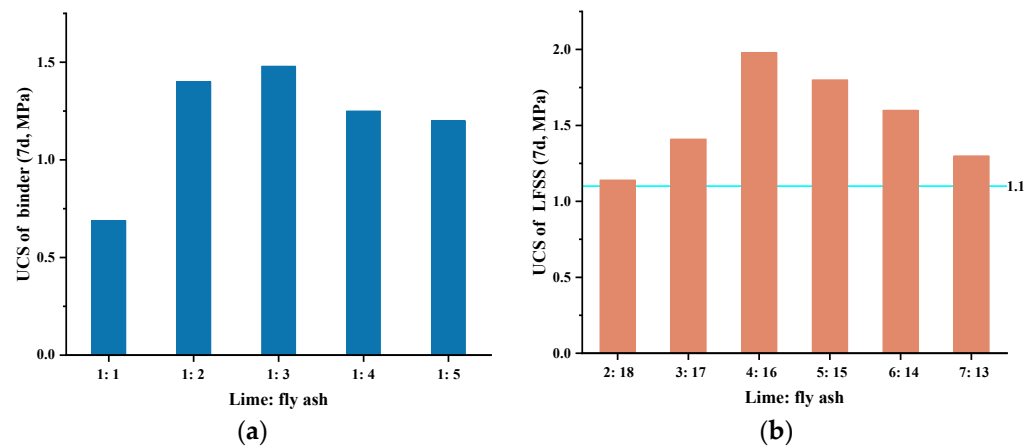


Figure 9. (a) UCS of binder; (b) UCS of LFSS; UCS of different binder of LFSS (binder-to-aggregate ratio= 1:4) (Adapted from [74]).

3.2.2. DS of LFSS

The water loss rate and DSC of LFSS are shown in Figure 10. Because all materials in LFSS have high water absorption, it shows significant water loss rate in the early stage. On the third day, the maximum water loss rate exceeded 5%. On average, the water loss rate in the first week exceeded 90% of the whole observation period, and the second week accounted for less than 10%. In comparison with CSS, LFSS exhibits less shrinkage deformation. The DS of LFSS is mainly affected by the water in SS and lime–fly ash. In general, the more the content of fine aggregate, lime and fly ash, the greater the DSC. In addition, the increase of dry density may also lead to the increase of DSC. Because the initial water content is high, mainly due to the rapid evaporation of free water, and the DS is less affected, and the DSC shows a downward trend.

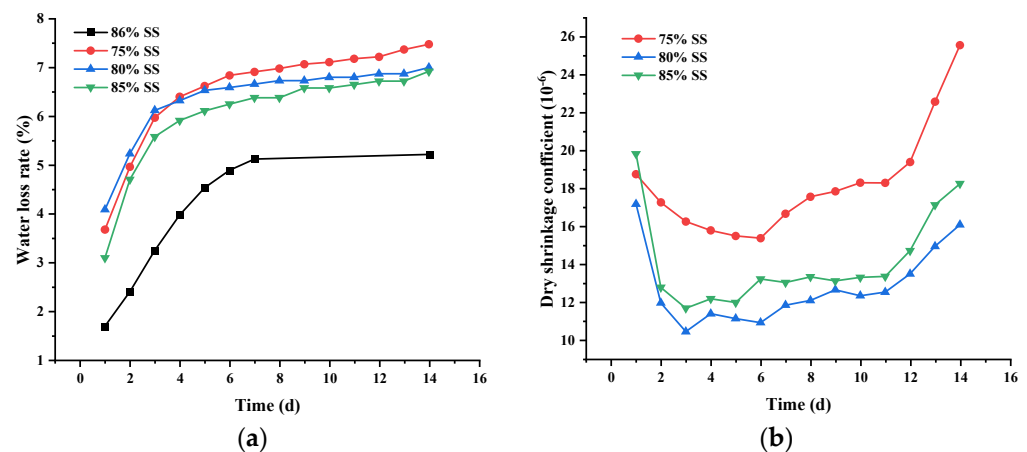


Figure 10. (a) The water loss rate of LFSS with curing time (lime-to-fly ash ratio = 1:3) (Adapted from [58,74]) (b) Dry shrinkage development of LFSS with different SS contents (Adapted from [74]).

3.2.3. TS of LFSS

The TS of lime–fly ash stabilized mixture is explained by the fact that each component of the material has thermal expansion and shrinkage when it meets heat and cold. There are many minerals in LFSS mixture, which can be mainly divided into aggregate and new cementitious minerals. The TSC varies between different materials. According to the existing study, the thermal expansion and shrinkage of new cement minerals is much greater than that of raw material minerals. Therefore, with the increase of SS in the mixture, the internal hydration products also increase, which improves the sensitivity of the mixture to temperature [76]. SS is more sensitive to temperature, which is consistent with the TS of CSS, as shown in Figure 11. The existing study results show that the TSC of LFSS

shows different trends. However, it is noteworthy that there are inflection points around 0–10 °C. From high temperature interval to low temperature interval, TSC first showed a downward trend, and then increased [74]. The maximum values of different SS contents appeared at between –10 and –20 °C. The maximum values of TSC were 130.8%, 84.3%, and 93.6% higher than the minimum values, respectively. According to Li, et al. [58], TSC first increased with temperature decrease, then decreased. The difference between the maximum value and the minimum value of TSC is only 21.4%. It indicated that the effect of temperature in CFSS is not significant. In general, the change trend of TSC is complex and needs to be further studied.

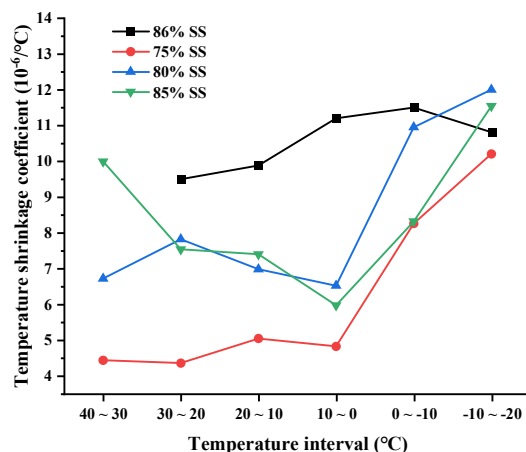


Figure 11. Temperature shrinkage of LFSS with different SS contents (Adapted from [58,74]).

3.3. Cement–Fly Ash Stabilized Steel Slag (CFSS)

In CFSS mixtures, the gradation and strength of the SS itself caused the SS skeleton to have a certain strength. In addition, among the SS particles, due to the active substances provided by cement hydration, physical and chemical reactions such as ion exchange reaction, Ca(OH)₂ crystallization reaction, and pozzolanic reaction are carried out in the water environment in the mixture. The main function of fly ash was to provide the active silica and alumina required for the pozzolanic reaction. The activity was stimulated by the action of cement and alkaline substances to promote the pozzolanic reaction. The reaction of cement fly ash in the mixture increased with age, and various reactions continued. The products generated by the pozzolanic reaction were aggregated, forming a chaotic spatial network connection between the SS particles, and the connection strength and stiffness were enhanced so that the CFSS had high strength. Components and properties of CFSS are shown in Table 5.

Table 5. Components and properties of CFSS from the researched literature.

Cement Content (%)	Fly Ash/SS Content (%)	OMC (%)	MDD (g/cm ³)	References
1/2/3/4	10/90, 20/80	7.90–10.10	2.31–2.63	[48]
4	0/100, 10/90, 20/80, 30/70, 40/60, 50/50, 60/40	7.00–15.80	1.64–2.30	[50]
2/4/6/8	0/100, 10/90, 20/80, 30/70, 40/60	-	-	[34]
4/6/8/10	36/60, 34/60, 32/60, 26/70, 24/70, 22/70, 20/70, 16/80, 14/80, 12/80, 10/80	15.30–23.20	1.53–1.84	[77]

3.3.1. OMC and MDD of CFSS

In Figure 12, the cement was calculated by external admixture. In CFSS mixtures, OMC was significantly larger than that of CSS mixtures due to the presence of fly ash. With the increase of cement content, both OMC and MDD showed an increasing trend.

From 1%–4%, OMC increased by approximately 5%, and MDD increased by 3% and 4%, respectively. Compared with cement, the change of SS content had a more significant effect on OMC and MDD. The SS content changed from 80% to 90%, and the OMC decreased by 21%–24%. The OMC was changed since the WA of fly ash was much larger than that of SS. Conversely, the specific gravity of SS was slightly larger than that of fly ash, so the addition of more SS led to an increase in the density of the mixture. Therefore, the SS content changed from 80% to 90%, and the MDD increased by 9%–11%. At the same compaction energy, the mixture was compacted to a higher density, resulting in an increase in MDD and a decrease in OMC. Therefore, replacing fly ash with an equivalent amount of SS will inevitably increase the dry density of CFSS.

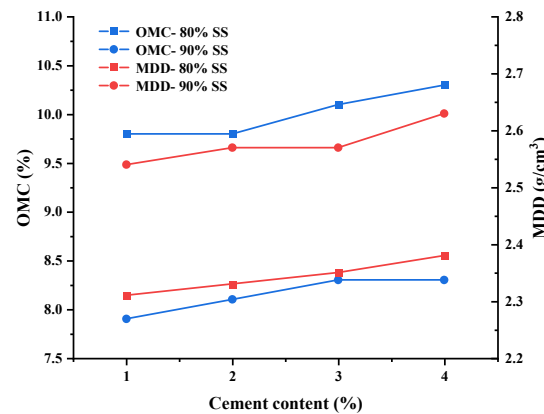


Figure 12. OMC, MDD with different SS and cement contents (Adapted from [48]).

3.3.2. UCS of CFSS

Figure 13a shows the UCS of CFSS at 4% cement content. Singh, et al. [34] and Yu [77] found the UCS development law of 0%–40% and 6%–80% SS content, respectively. The results showed that with the increase of SS, the UCS increases continuously. Zhou, et al. [50] found that with the increase of fly ash content, the UCS of CFSS first increased and then decreased. When the content of SS was 80%, the UCS reached the maximum value. In the mixtures, the cement provided the active substance, prompting the crystallization reaction of $\text{Ca}(\text{OH})_2$, the pozzolanic reaction, and other reactions. Fly ash provided the active silica and alumina required for the pozzolanic reaction. The activity was stimulated under the action of cement and alkaline substances to promote the pozzolanic reaction.

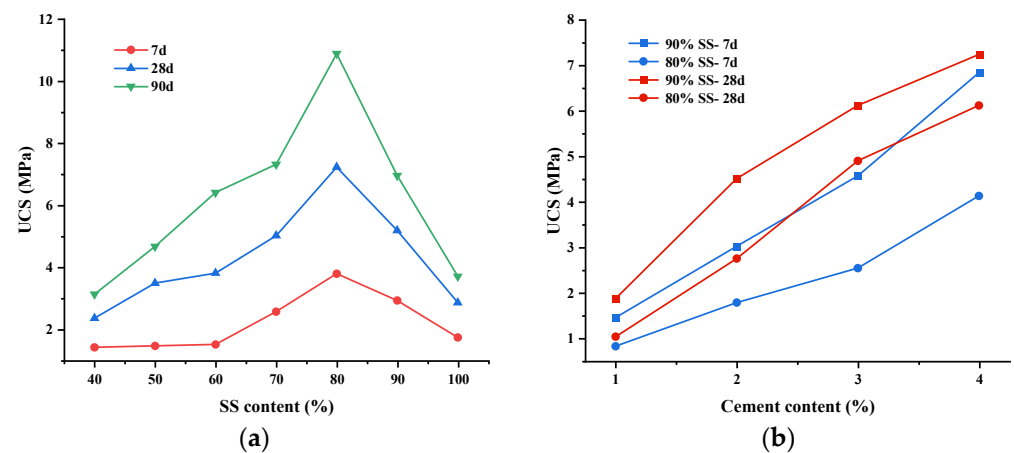


Figure 13. (a) The effect of fly ash addition on the UCS of CFSS (Adapted from [50]) (b) The effect of cement contents on the UCS of CFSS (Adapted from [48]).

Compared with no addition of fly ash (100% SS), the incorporation of 20% fly ash (80% SS) increased the 7d, 28d, and 90d UCS of CFSS by 126%, 157%, and 197%, respectively [50].

This can be explained by the fact that the surface of the SS particles without fly ash had a thin binder coating, resulting in a small contact area between the SS particles. In this case, it was easy to cause stress concentration and damage under pressure. With the addition of fly ash, the thickness of the binder coating gradually increased, making it increasingly dispersed and subject to compressive stress.

The compressive strength of CFSS increased with curing time. The reaction of cement fly ash in the mixture continues with the curing time, and the amount of the generated cementitious substances also increases. This made a strong connection between the SS particles, and the strength and stiffness of the association were gradually increased so that the compressive strength of the CFSS was also gradually increased.

With the increase of cement content, UCS of CFSS also increases as shown in Figure 13b. This can be explained by the fact that the increase of curing time and binder content will increase the amount of C-S-H gel, thus improving the compressive strength of the mixture. In the case of the same cement content, the compressive strength was also significantly improved by adding SS. SS could therefore play a role in increasing bearing load and providing strength, which improved the UCS of CFSS.

3.3.3. DS of CFSS

Figure 14 reflects the relationship between moisture loss rate and curing time. The moisture loss rate of the mixture increased with time. In the first ten days, the water loss rate was faster, and its curve increased almost linearly. As the moisture content in the mixture was consistent with the surrounding environment, the average moisture loss hardly changed. In addition, there was also a certain relationship between the moisture loss rate and the OMC of the mixture. The greater the OMC of the mixture, the greater the water loss rate.

The DSC decreased with curing time. As shown in Figure 15a, the maximum values of DSC for different blend ratios all appeared in the early stage. This was the reason for the enormous DS strain of the mixture in the early stage. From approximately the eighth day, the DSC began to tend to the level and maintained at around 122×10^{-6} , 94×10^{-6} , and 101×10^{-6} , respectively [77]. Compared to the first day, DSC decreased by 64%, 68%, and 51%, respectively. With the increase of SS content, the DSC decreased to a certain extent. For example, in the previous week of curing time, the DSC of 80% SS was more significant than that of 70% SS. The changes in DSC and cement content after the seventh day are shown in Figure 15b, when the content of SS was 70%. During the first week, the regularity of DSC development was not significant, but after a week, the mixture with lower cement content and more fly ash showed less DS. Among them, the DSC difference of 8% cement content and 10% mixture was not significant.

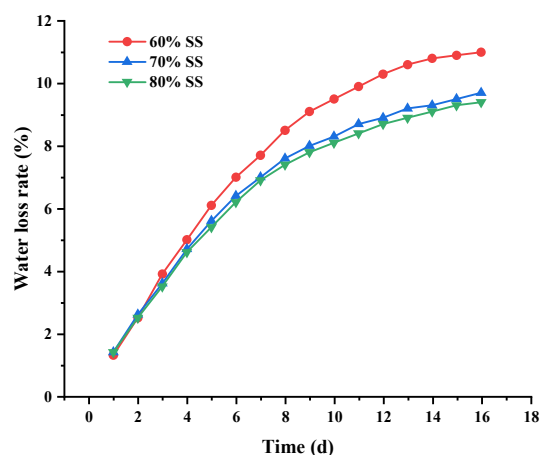


Figure 14. The water loss rate of LFSS with curing time (6% cement) (Adapted from [77]).

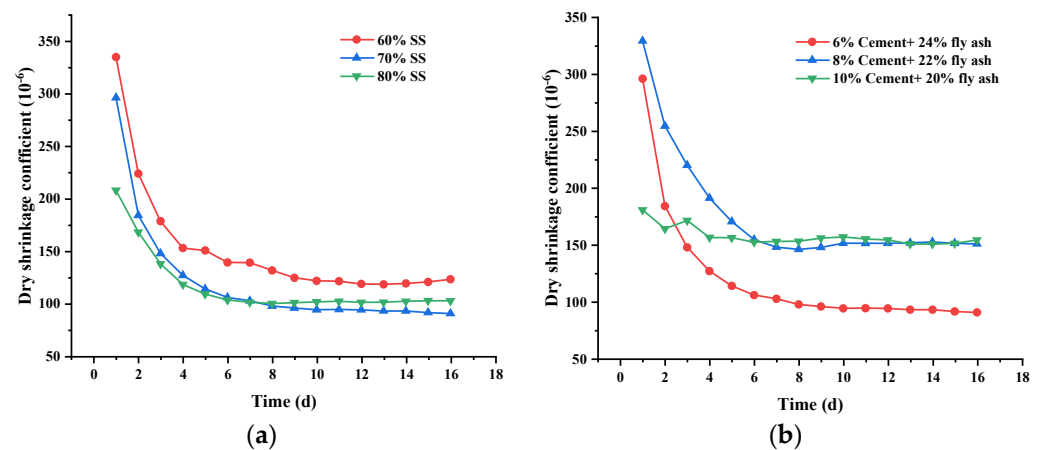


Figure 15. (a) different SS content; (b) different cement and fly ash contents; Dry shrinkage development of CFSS (Adapted from [77]).

3.3.4. Inhibition Mechanism of Fly Ash on CFSS

Figure 16 showed the SEM image results of the side of the cement–fly ash binder in contact with the SS. The results showed that many needle-like, fibrous, and sheet-like C-S-H phases were formed on the surface of the binder [50]. The hydration of f-CaO in SS did not form larger $\text{Ca}(\text{OH})_2$ crystals [56]. The increase of fly ash content reduced the possibility of SS forming a skeleton and prevented the concentration of expansion stress between SS. The low elastic modulus of the cement–fly ash binder relieved the expansion stress formed by the $\text{Ca}(\text{OH})_2$ expansion component. The binder reacted with the products produced by the expansion of the SS, preventing the further growth of $\text{Ca}(\text{OH})_2$ [78,79].

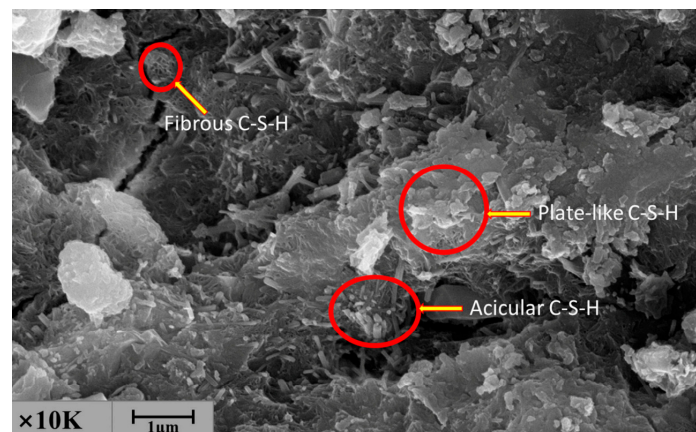


Figure 16. The SEM analysis of the binder on the side where the binder contacted and SS (Adapted from [50]).

4. Numerical Simulation

With the rapid development of computer hardware and related scientific theories, numerical simulation technology has been widely used in materials research, such as finite element method (FEM), discrete element method (DEM), and molecular dynamics (MD) [18,39,80–84]. The experimental cost of CSS is relatively large, the testing period is long, and there are many uncontrollable external factors. Therefore, numerical simulation technology has been adopted by some scholars in the study of CSS.

Wu [83] conducted a freeze–thaw cycle test on CSS specimens to consider the damage to the CSS base in a seasonally frozen area. A simulation model of the freeze–thaw cycle test suitable for CSS was constructed using ANSYS Workbench. Through the numerical comparison analysis of the compressive strength test and simulation undergoing different

freezing and thawing cycles (0, 5, 10, 20 times), it was found that the accuracy exceeded 92%. Through the numerical simulation of the freeze–thaw cycle test of CSS specimens, the results showed that the stress and strain change periodically with temperature and are positively correlated. With the increase of freezing and thawing times, the specimens were subjected to stress and gradually diffused inward. The maximum stress on the inside and outside of the samples increased accordingly. By comparing and calculating the temperature, stress, and strain of each pavement structure with and without bed course, it was recommended to set a cushion to protect the CSS in low-temperature areas.

Karatağ, et al. [18] used Plaxis software to perform a plane-strain FEM analysis of the rutting characteristics of the SS base. A hardening soil model with small-strain stiffness was used to examine the deformation behavior of layered pavement whereas asphalt concrete modeled using the linear elastic model. After 10,110 triangular load cycles, the rutting rate of the asphalt pavement on the SS base was approximately 33% lower than that on the gravel base. It could be seen that SS was a better substitute for natural aggregate in terms of deformation properties.

MD is an emerging technology to describe interactions between substances [85–87]. MD simulation has been widely used in materials science, biology, medicine, physical chemistry, and other fields [88]. Liu, et al. [39] selected the condensed-phase optimized molecular potentials for atomistic simulation study for cement–water–SS interfacial simulation. The results showed that the interfacial binding energy of the SS mixture reached 2781.6 MJ/m², which was much larger than that of limestone (830.5 MJ/m²). Since both limestone and SS are alkaline stones, Coulomb electrostatic interactions account for most of the interfacial binding energy. A total of 91.80% of the cement–limestone interfacial energy was composed of electrostatic energy, and in the cement–SS system, the electrostatic energy increases to 99.55%. It could be concluded that during the stirring process, due to the large positive charge contained in the SS, the electrostatic energy increased, resulting in enhanced adhesion between the cement and the SS. At the same time, the displacement velocity of the particles indicated that the diffusion rate of cement molecules in the SS mixture was faster than that of limestone. This showed that the cement wrapped the SS earlier and underwent hydration, which was beneficial to forming the early strength of the SS mixture.

Wang, et al. [84] argued that traditional finite element methods focused on the macroscopic behavior of materials, while ignoring the evolution of the microstructure. Therefore, based on 3D scanning technology and in combination with physical test results, a DEM of CSS with actual SS shape was constructed using Particle Flow Code 3D. During the CSS failure process, microcracks went through four stages: initiation, propagation, convergence, and penetration, as shown in Figure 17. The leading cause of CSS failure was the absorption and dissipation of energy within the structure. With the increase of SS content, the number of microcracks gradually increased and the width of the crack surface increased after the failure of the specimen. It was worth noting that the SS content, SS particle size, SS roughness, and interface tensile strength had a great influence on the CSS interface transition zone.

FEM, DEM, and MD have been adopted in different scales for SS base simulation research, but they are still in the exploratory stage. FEM and DEM are mainly used to simulate the cracks, rutting, freeze–thaw, anti-scour, and so on. MD is often selected to simulate the diffusion of binder in the mixture to analyze the strength formation mechanism. Numerical simulation results cannot be well connected with mechanical properties and durability, so they cannot be well applied.

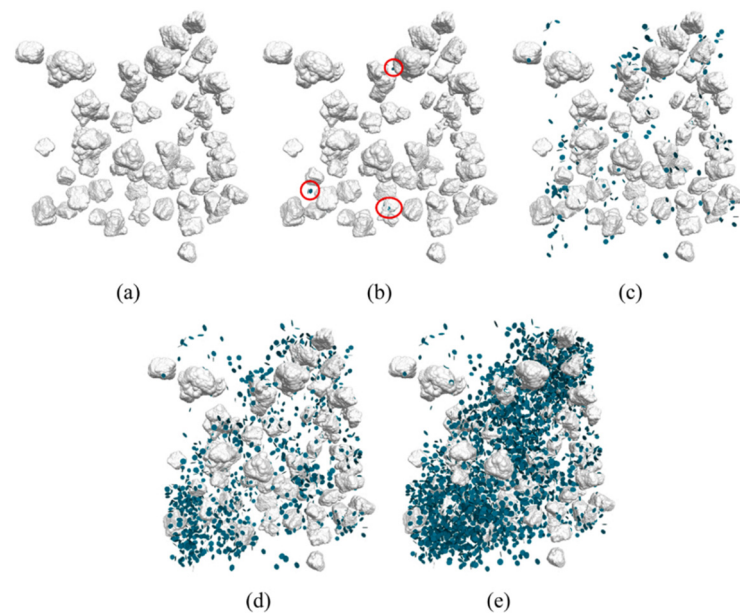


Figure 17. Crack evolution process of CSS (a) original model (b) initiation (c) expansion (d) convergence (e) penetration (Reprinted with permission from [84] Copyright Elsevier).

5. Environmental Impacts

Road engineering is one of the major consumers of natural resources [89,90] and one of the major producers of CO₂ emissions [91,92]. Life cycle assessment (LCA) is a set of standard procedures for evaluating environmental–economic efficiency in engineering with the aim of finding better alternatives [93]. Based on the LCA assessment, the utilization of SS has considerable environmental benefits [94]. Researchers have demonstrated that SS utilization can significantly reduce greenhouse gases and ecological impacts [94,95]. Kang, et al. [96] build a SS prediction model based on a convolutional neural network by relying on a big data acquisition and storage system to recommend the optimal utilization of SS.

Anastasiou, et al. [97] evaluated the pavement construction with fly ash as binder and SS as aggregate. Fly ash can significantly reduce the environmental impact of road construction, of which binder replacement rate is the most crucial factor. The environmental benefits of replacing 50% of cement with fly ash are far greater than the long-distance transportation of fly ash [98]. The CO₂ emissions of long-distance transport aggregates are similar, and they account for a small proportion of the total emissions from road construction. SS as aggregate can minimize the consumption of ecological resources, but it is not recommended to transport SS over long distances.

Liu, et al. [39] evaluated CO₂ emissions from material production and transportation for CSM and CSS at 50% SS. The results showed that due to the large power consumption in the cement production process, the emission of CO₂ accounts for the largest proportion. The transport emissions of SS and gravel mixture accounted for 28.9% and 19.3% of the total emissions, respectively. Throughout the process, CSS (188, 368 kg) produced 0.25% more CO₂ than CSM (187, 896 kg).

Gao, et al. [38] discussed the compaction process of SS base and andesite (a natural aggregate) base. The 98% compaction degree in the standard is used as the evaluation index [99]. Based on the comparison of the three compaction methods, the results show that strong vibration should be avoided or reduced and the static pressure exerted by the roller compactor should be increased during SS compaction. This approach mitigates the unfavorable “hard-to-hard” effect between adjacent slag particles, as shown in Figure 18. The “hard-to-hard” effect refers to the deformation of SS particles under strong vibration, followed by continuous elastic recovery and expansion. The final SS particle gap is more significant than the initial one, which leads to a decrease in the density of the mixture after

compaction. Compared with the andesite base, the diesel consumption of the compactor at the SS base is higher, the energy consumption increases by 2.67 MJ/m^3 , and the CO_2 equivalent emission increases by 0.20 kg/m^3 .

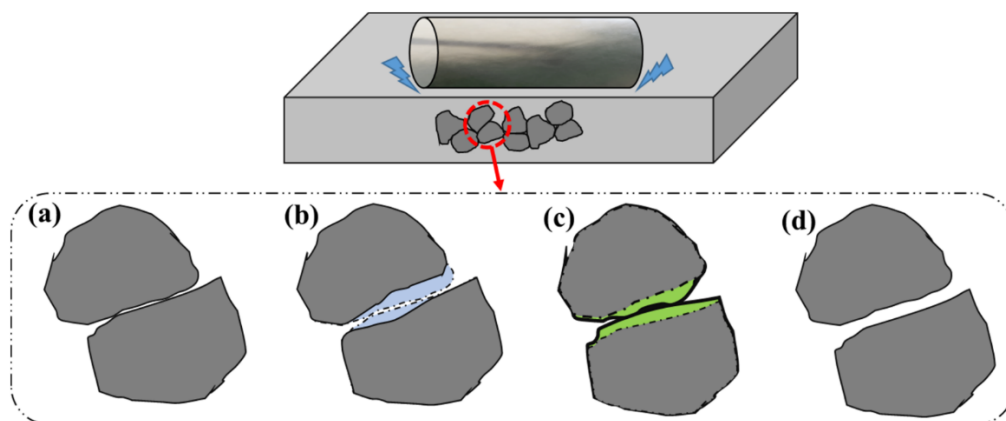


Figure 18. “Hard-to-hard” effect in SS compaction (a) the particles close to each other (b) deformation under external strong vibration (c) an elastic recovery expansion (d) the displacement of the particles results in a macroscopic decrease in density (Adapted from [38]).

At present, the environmental impact assessment of SS base mainly focuses on transportation and compaction. From the perspective of construction economic cost, it is recommended to use SS only in a short distance, and the environmental benefits generated by higher content of solid waste will be more significant. For the compaction process of road base, the CO_2 emission of SS base course is slightly more than that of traditional base.

6. Conclusions

This paper focuses on a critical on the utilization of SS as a road material in semi-rigid base course. The physical, mechanical, and durability properties indicate that SS is suitable for semi-rigid base. It is usually the basic performance of SS that is considered when used for semi-rigid base, rather than its production process. However, it is essential to pay attention to the high-water absorption and calcium oxide content of SS.

The utilization of SS as a road base material in the literature can be mainly classified into three aspects, consisting of CSS, LFSS, and CFSS. The SS content will significantly increase OMC and MDD in CSS. The gradation of CSS will affect OMC, but has little effect on MDD. The UCS rises with the SS content increasing. The water loss rate and DSC showed a similar growth trend as time increases. The increase of SS and cement content will increase the water loss rate, and DSC shows the opposite trend. After the addition of SS, the TSC of the mixture rises, but the increased value is far less than the decrease of DSC, which reduces the DS of the base course. In LFSS, when the content ratio of lime-to-fly ash is 1:3, the maximum strength is achieved, and this proportion is recommended. The ratio of binder-to-SS will also have a significant impact on UCS values, and around 20:80 is recommended. Due to the slow pozzolanic reaction, the increase of curing time can significantly improve the UCS value. In comparison with CSS, LFSS exhibits less DS deformation. The law of TSC is not clear, but there is an inflection point between $0\text{--}10\text{ }^\circ\text{C}$. In CFSS, the change of SS content has a more significant impact on OMC and MDD than that of cement content. The UCS increases with the increase of SS content, and there may be an optimal content. Cement, fly ash, and curing time have a positive effect on the UCS. As time increases, DSC decreases continuously, and large DS strains will be apparent during the early stage of the mixture. There is no obvious correlation between DSC and the content of cement and fly ash. FEM, DEM, and MD can be used to analyze the freeze–thaw, rutting resistance, and crack development of SS base. LCA is used to evaluate SS road base, which shows significant environmental significance. However, the CO_2 equivalent emission of SS

base in the process of production, transportation, and construction is slightly higher than that of the traditional macadam base.

Based on this overview, the authors believe that further research is needed in certain directions so as to promote the application of SS as a road material in semi-rigid base:

(1) The SS base course is generally designed according to the traditional grading range recommended in the specification, and the particle size is within 0–31.5 mm. However, the particle size of SS produced in the iron and steel industry is too large, and secondary crushing is often required for the base course. After that, the SS mixture meets the requirements in various properties, and the gradation of SS itself is not fully utilized. If the grading design method based on the original grading of SS can be put forward, it will better promote the application of SS in the base course. In addition, the structural type is less considered, and it is not clear how the structural type affects the performance in the SS base.

(2) With the significant improvement of mechanical level and field construction technology, more projects adopt large thickness one-time molding to ensure the quality of road construction. However, in the laboratory test, heavy compaction and static pressure forming method are still widely used. It is worth noting that this method is matched with the static roller and cannot effectively guide the gradation design and field construction of a large thickness SS base course. In the laboratory test, it is necessary to select appropriate test methods of SS base to better simulate the field construction, so as to ensure the authenticity and reliability of the design results. At the same time, most of the existing studies focus on the mechanical properties, DS, and TS of the mixture, and there is little research on the anti-scour, fatigue performance, and frost resistance of the mixture. The applicability of SS base in rainy and cold areas is not clear.

(3) Moreover, it is time-consuming and expensive to test the performance of SS base course, and there are numerous uncontrollable factors. The numerical simulation of SS base course will be one of the important research directions in the future, but now the numerical simulation of SS base is still in the initial stage of development, and FEM, DEM, and MD have been adopted by researchers. How to combine numerical simulation with experimental characterization to explain the macro and micro mechanism and predict the performance of SS mixture remains to be explored. Meanwhile, based on LCA, the whole process of raw materials production, transportation, base course paving and use, and even abandonment needs to be evaluated. However, there is little research on the paving and using process of SS base. In addition to the compaction process, the high strength, high capacity and high-water absorption of SS will have different effects on the mixing and paving of the mixture. The impact of SS base on the environment has yet to be assessed.

Author Contributions: H.L.: conceptualization, methodology, validation, investigation, writing—original draft. C.C.: conceptualization, writing—review and editing. J.C.: supervision, project administration, resources, funding acquisition. M.Z.: methodology, writing—review and editing. Y.S.: writing—review and editing, supervision. All authors have read and agreed to the published version of the manuscript.

Funding: This research was funded by Key R & D and Transformation Plan of Qinghai Province (2021-SF-165), Key Research and Development Project of Shaanxi Province (2022SF-328), the Science and Technology Project of Henan Department of Transportation (2020J-2-3), Science and Technology Project of Shaanxi Department of Transportation (No.19-10K, No.19-28K).

Institutional Review Board Statement: Not applicable.

Informed Consent Statement: Not applicable.

Data Availability Statement: The information used to bolster the discoveries of this research are from prior detailed studies cited before.

Acknowledgments: We express our sincere gratitude to the experts, teachers, and students who have provided help for this article.

Conflicts of Interest: The authors declare no conflict of interest.

Abbreviations

ASG	Apparent specific gravity	LA	Los Angeles abrasion
CFSS	Cement–fly ash stabilized steel slag	LCA	Life cycle assessment
C-S-H	Calcium silicate hydrates	LFSS	Lime–fly ash stabilized steel slag
CSM	Cement stabilized macadam	MD	Molecular dynamics
CSS	Cement stabilized steel slag	MDD	Maximum dry density
CV	Crushing value	OMC	Optimum moisture content
DEM	Discrete element method	SS	Steel slag
DS	Drying shrinkage	TS	Temperature shrinkage
DSC	Drying shrinkage coefficient	TSC	Temperature shrinkage coefficient
EFP	Elongated and flaky particles	UCS	Unconfined compressive strength
FEM	Finite element method	WA	Water absorption

References

- Li, B.; Tang, B.; Ma, Z.; Cheng, H.; Li, H. Physical and chemical properties of steel slag and utilization technology of steel slag at home and abroad. In Proceedings of the IOP Conference Series: Earth and Environmental Science, Moscow, Russia, 27 May–6 June 2019; p. 032012.
- Song, Q.; Guo, M.; Wang, L.; Ling, T. Use of steel slag as sustainable construction materials: A review of accelerated carbonation treatment. *Resour. Conserv. Recycl.* **2021**, *173*, 105740. [[CrossRef](#)]
- Gu, X.; Yu, B.; Dong, Q.; Deng, Y. Application of secondary steel slag in subgrade: Performance evaluation and enhancement. *J. Clean. Prod.* **2018**, *181*, 102–108. [[CrossRef](#)]
- Gençel, O.; Karadag, O.; Oren, O.H.; Bilir, T. Steel slag and its applications in cement and concrete technology: A review. *Constr. Build. Mater.* **2021**, *283*, 122783. [[CrossRef](#)]
- Hayashi, A.; Watanabe, T.; Kaneko, R.; Takano, A.; Takahashi, K.; Miyata, Y.; Matsuo, S.; Yamamoto, T.; Inoue, R.; Ariyama, T. Decrease of Sulfide in Enclosed Coastal Sea by Using Steelmaking Slag. *Tetsu-to-Hagane* **2012**, *98*, 207–214. [[CrossRef](#)]
- Wang, Z.; Sohn, I. A review on reclamation and reutilization of ironmaking and steelmaking slags. *J. Sustain. Metall.* **2019**, *5*, 127–140. [[CrossRef](#)]
- Gao, X.; Okubo, M.; Maruoka, N.; Shibata, H.; Ito, T.; Kitamura, S.-Y. Production and utilisation of iron and steelmaking slag in Japan and the application of steelmaking slag for the recovery of paddy fields damaged by Tsunami. *Miner. Process. Extr. Metall.* **2015**, *124*, 116–124. [[CrossRef](#)]
- Semykina, A.; Shatokha, V.; Seetharaman, S. Innovative approach to recovery of iron from steelmaking slags. *Ironmak. Steelmak.* **2010**, *37*, 536–540. [[CrossRef](#)]
- Wang, X.; Li, X.; Yan, X.; Tu, C.; Yu, Z. Environmental risks for application of iron and steel slags in soils in China: A review. *Pedosphere* **2021**, *31*, 28–42. [[CrossRef](#)]
- Yu, H.; Ma, T.; Wang, D.; Wang, C.; Lu, S.; Zhu, X. Review on China’s pavement engineering research·2020. *China J. Highw. Transp.* **2020**, *33*, 1–66.
- Guo, J.; Bao, Y.; Wang, M. Steel Slag in China: Treatment, Recycling, and Management. *Waste Manag.* **2018**, *78*, 318–330. [[CrossRef](#)]
- Yildirim, I.Z.; Prezzi, M. Chemical, Mineralogical, and Morphological Properties of Steel Slag. *Adv. Civ. Eng.* **2011**, *2011*, 463638. [[CrossRef](#)]
- Motz, H.; Geiseler, J. Products of steel slags an opportunity to save natural resources. *Waste Manag.* **2000**, *21*, 285–293. [[CrossRef](#)]
- Yi, H.; Xu, G.; Cheng, H.; Wang, J.; Wan, Y.; Chen, H. An overview of utilization of steel slag. *Procedia Environ. Sci.* **2012**, *16*, 791–801. [[CrossRef](#)]
- Riley, A.L.; MacDonald, J.M.; Burke, I.T.; Renforth, P.; Jarvis, A.P.; Hudson-Edwards, K.A.; McKie, J.; Mayes, W.M. Legacy iron and steel wastes in the UK: Extent, resource potential, and management futures. *J. Geochem. Explor.* **2020**, *219*, 106630. [[CrossRef](#)]
- Behiry, A.E.A.E.-M. Evaluation of steel slag and crushed limestone mixtures as subbase material in flexible pavement. *Ain Shams Eng. J.* **2013**, *4*, 43–53. [[CrossRef](#)]
- Kumar, P.; Kumar, A. Steel industry waste utilisation in road sector of India. *J. Inst. Eng. (India) Civ. Eng. Div.* **2000**, *80*, 182–185.
- Karatağ, H.; Firat, S.; Işık, N.S. Assessment of performance of steel slag used in road base by finite element analysis. In Proceedings of the 13th International Congress on Advances in Civil Engineering, Izmir, Turkey, 12–14 September 2018.
- Pasetto, M.; Baldo, N. Mix design and performance analysis of asphalt concretes with electric arc furnace slag. *Constr. Build. Mater.* **2011**, *25*, 3458–3468. [[CrossRef](#)]
- Pasetto, M.; Baldo, N. Influence of the aggregate skeleton design method on the permanent deformation resistance of stone mastic asphalt. *Mater. Res. Innov.* **2014**, *18*, S3-96–S3-101. [[CrossRef](#)]
- Bessa, I.S.; Castelo Branco, V.T.F.; Soares, J.B. Evaluation of polishing and degradation resistance of natural aggregates and steel slag using the aggregate image measurement system. *Road Mater. Pavement Des.* **2014**, *15*, 385–405. [[CrossRef](#)]
- Wu, S.; Cui, P.; Xie, J.; Liu, Q.; Pang, L. Expansive inhibition method of steel slag aggregate and volume stability of mixture: A review. *China J. Highw. Transp.* **2021**, *34*, 166–179.
- Sha, A. Material characteristics of semi-rigid base. *China J. Highw. Transp.* **2008**, *21*, 1.

24. JTG/T F20-2015; Technical Guidelines for Construction of Highway Roadbases. Ministry of Transport of the People's Republic of China: Beijing, China, 2015.
25. Deng, C.; Jiang, Y.; Tian, T.; Chen, Z. Resilient modulus and influencing factors of vertical vibration compacted cement-stabilized macadam. *Int. J. Pavement Eng.* **2021**, *22*, 1435–1445. [CrossRef]
26. Deng, C.; Jiang, Y.; Lin, H.; Ji, X. Mechanical-strength-growth law and predictive model for cement-stabilized macadam. *Constr. Build. Mater.* **2019**, *215*, 582–594. [CrossRef]
27. Mallela, J.; Quintus, H.V.; Smith, K. Consideration of lime-stabilized layers in mechanistic-empirical pavement design. *Natl. Lime Assoc.* **2004**, *200*, 1–40.
28. Xue, J.; Jiang, Y. Analysis on the fatigue properties of vertical vibration compacted lime-fly ash-stabilized macadam. *Constr. Build. Mater.* **2017**, *155*, 531–541. [CrossRef]
29. Deng, C.; Jiang, Y.; Yuan, K.; Tian, T.; Yi, Y. Mechanical properties of vertical vibration compacted lime-fly ash-stabilized macadam material. *Constr. Build. Mater.* **2020**, *251*, 119089. [CrossRef]
30. Lav, A.H.; Lav, M.A.; Goktepe, A.B. Analysis and design of a stabilized fly ash as pavement base material. *Fuel* **2006**, *85*, 2359–2370. [CrossRef]
31. Liu, Z.; Guan, D.; Moore, S.; Lee, H.; Su, J.; Zhang, Q. Climate policy: Steps to China's carbon peak. *Nature* **2015**, *522*, 279–281. [CrossRef]
32. Cetin, B.; Aydilek, A.H.; Guney, Y. Stabilization of recycled base materials with high carbon fly ash. *Resour. Conserv. Recycl.* **2010**, *54*, 878–892. [CrossRef]
33. Ferreira, C.; Ribeiro, A.; Ottosen, L. Possible applications for municipal solid waste fly ash. *J. Hazard. Mater.* **2003**, *96*, 201–216. [CrossRef]
34. Singh, S.; Tripathy, D.P.; Ranjith, P.G. Performance evaluation of cement stabilized fly ash-GBFS mixes as a highway construction material. *Waste Manag.* **2008**, *28*, 1331–1337. [CrossRef] [PubMed]
35. Mallick, R.B.; Hendrix, G., Jr. Use of foamed asphalt in recycling incinerator ash for construction of stabilized base course. *Resour. Conserv. Recycl.* **2004**, *42*, 239–248. [CrossRef]
36. Sun, Y.; Li, L. Strength assessment and mechanism analysis of cement stabilized reclaimed lime-fly ash macadam. *Constr. Build. Mater.* **2018**, *166*, 118–129. [CrossRef]
37. Li, Q.; Wang, Z.; Li, Y.; Shang, J. Cold recycling of lime-fly ash stabilized macadam mixtures as pavement bases and subbases. *Constr. Build. Mater.* **2018**, *169*, 306–314. [CrossRef]
38. Gao, B.; Yang, C.; Zou, Y.; Wang, F.; Zhou, X.; Barbieri, D.; Wu, S. Compaction Procedures and Associated Environmental Impacts Analysis for Application of Steel Slag in Road Base Layer. *Sustainability* **2021**, *13*, 4396. [CrossRef]
39. Liu, J.; Yu, B.; Wang, Q. Application of steel slag in cement treated aggregate base course. *J. Clean. Prod.* **2020**, *269*, 121733. [CrossRef]
40. Li, W.; Lang, L.; Lin, Z.; Wang, Z.; Zhang, F. Characteristics of dry shrinkage and temperature shrinkage of cement-stabilized steel slag. *Constr. Build. Mater.* **2017**, *134*, 540–548. [CrossRef]
41. Xiao, J.; Long, C.; He, J.; Chang, J.; Wu, C.; Liu, C.; Yan, W. Performance and micro characteristics of cement stabilized macadam with a large amount of Activated steel slag powder. *China J. Highw. Transp.* **2021**, *34*, 204.
42. Li, Q.; Li, B.; Li, X.; He, Z.; Zhang, P. Microstructure of pretreated steel slag and its influence on mechanical properties of cement stabilized mixture. *Constr. Build. Mater.* **2022**, *317*, 125799. [CrossRef]
43. Yoshida, N. Uniaxial compressive strength of hydraulic, graded iron and steel slag base-course material produced at different manufacturers and its increase with curing time. In Proceedings of the 15th Asian Regional Conference on Soil Mechanics and Geotechnical Engineering, ARC 2015, Fukuoka, Japan, 9–13 November 2015; pp. 1614–1618.
44. Li, C.; Xiang, X.; Liu, S.; Hua, Z.; Jiao, L. Experimental research on the basic performance of the semi-rigid base material with steel-slag. *Multipurp. Util. Miner. Resour.* **2015**, *3*, 73–77.
45. Li, W.; Lang, L.; Wang, Z.; Chen, J. Experimental research on cracking performance of semi-rigid steel slag base. *Constr. Technol.* **2017**, *46*, 47–52.
46. Ji, X.; Sheng, Y.; Lu, Z.; Xin, D.; Long, Y.; Chen, H. Properties of semi-rigid base material with steel slag. *J. Chang. Univ.* **2021**, *41*, 21–31.
47. Yang, Y.; Tan, B.; Li, Y.; Liu, Q. Preparation and properties of water stabilized base material of refined steel slag based on alkali excitation. *J. Guilin Univ. Technol.* **2021**, 1–8. Available online: <http://kns.cnki.net/kcms/detail/45.1375.N.20211221.1348.002.html> (accessed on 6 July 2022).
48. Lu, F.; Li, J. Application of Jinan Steel's converter slag in pavement base. *Highway* **2013**, *08*, 262–266.
49. Zeng, M.; Wu, S.; Hu, B.; Sun, Y.; Long, S. Experimental study on steel slag-crushed stone pavement base materials stabilized with portland cement. *Nat. Sci. J. Xiangtan Univ.* **2011**, *33*, 29–33.
50. Zhou, M.; Cheng, X.; Chen, X. Studies on the Volumetric Stability and Mechanical Properties of Cement-Fly-Ash-Stabilized Steel Slag. *Materials* **2021**, *14*, 495. [CrossRef]
51. O'Connor, J.; Nguyen, T.B.T.; Honeyands, T.; Monaghan, B.; O'Dea, D.; Rinklebe, J.; Vinu, A.; Hoang, S.A.; Singh, G.; Kirkham, M. Production, characterisation, utilisation, and beneficial soil application of steel slag: A review. *J. Hazard. Mater.* **2021**, *419*, 126478. [CrossRef]
52. Yildirim, I.; Prezzi, M. *Use of Steel Slag in Subgrade Applications*; Publication FWA: West Lafayette, Indiana, 2009.

53. Shi, C. Steel slag—Its production, processing, characteristics, and cementitious properties. *J. Mater. Civ. Eng.* **2004**, *16*, 230–236. [[CrossRef](#)]
54. Kandhal, P.S.; Hoffman, G.L. Evaluation of steel slag fine aggregate in hot-mix asphalt mixtures. *Transp. Res. Rec.* **1997**, *1583*, 28–36. [[CrossRef](#)]
55. Frías, M.; De Rojas, M.S.; Uría, A. Study of the instability of black slags from electric arc furnace steel industry. *Mater. Constr.* **2002**, *52*, 79–83. [[CrossRef](#)]
56. Wang, Q.; Wang, D.; Zhuang, S. The soundness of steel slag with different free CaO and MgO contents. *Constr. Build. Mater.* **2017**, *151*, 138–146. [[CrossRef](#)]
57. Barišić, I.; Dimter, S.; Rukavina, T. Elastic properties of cement-stabilised mixes with steel slag. *Int. J. Pavement Eng.* **2015**, *17*, 753–762. [[CrossRef](#)]
58. Li, F.; Chen, Y.; Gao, F.; Sun, Y.; Wu, C. Experiment and study on dry and temperature induced shrinkage properties of inorganic binder stabilized pavement base material with steel slag. *Highway* **2012**, *12*, 186–191.
59. Pai, R.R.; Bakare, M.D.; Patel, S.; Shahu, J.T. Structural Evaluation of Flexible Pavement Constructed with Steel Slag–Fly Ash–Lime Mix in the Base Layer. *J. Mater. Civ. Eng.* **2021**, *33*, 04021097. [[CrossRef](#)]
60. Jiang, Y.; Ling, T.; Shi, C.; Pan, S. Characteristics of steel slags and their use in cement and concrete—A review. *Resour. Conserv. Recycl.* **2018**, *136*, 187–197. [[CrossRef](#)]
61. Lun, Y.; Zhou, M.; Cai, X.; Xu, F. Methods for improving volume stability of steel slag as fine aggregate. *J. Wuhan Univ. Technol. Sci. Ed.* **2008**, *23*, 737–742. [[CrossRef](#)]
62. Zheng, W. *Application of Steel Slag in Cement Stabilized Crushed Stone Base*; Chang’an University: Xi’an, China, 2018.
63. *JTG D50-2017*; Specifications for Design of Highway Asphalt Pavement. Ministry of Transport of the People’s Republic of China: Beijing, China, 2017.
64. Wu, S. *Experimental Study on Steel Slag–Crushed Stone Pavement Base Materials Stabilized with Portland Cement*; Hunan University: Changsha, China, 2011.
65. Patel, S.; Shahu, J. Resilient response and permanent strain of steel slag-fly ash-dolime mix. *J. Mater. Civ. Eng.* **2016**, *28*, 04016106. [[CrossRef](#)]
66. Wang, Q.; Yan, P. Early hydration characteristics and paste structure of complex binding material containing high-volume steel slag. *J. Chin. Ceram. Soc.* **2008**, *36*, 1406–1411.
67. Wang, Q.; Yan, P.; Han, S. The influence of steel slag on the hydration of cement during the hydration process of complex binder. *Sci. China Technol. Sci.* **2011**, *54*, 388–394. [[CrossRef](#)]
68. Zhuang, S.; Wang, Q. Inhibition mechanisms of steel slag on the early-age hydration of cement. *Cem. Concr. Res.* **2020**, *140*, 106283. [[CrossRef](#)]
69. Wang, G.; Wang, Y.; Gao, Z. Use of steel slag as a granular material: Volume expansion prediction and usability criteria. *J. Hazard. Mater.* **2010**, *184*, 555–560. [[CrossRef](#)] [[PubMed](#)]
70. Xu, B. *Application of Steel Slag in Cement-Stabilized Macadam Base*; Changsha University of Science and Technology: Changsha, China, 2017.
71. Zeng, M.; Ruan, W.; Meng, Y.; Lin, C. Design and performance of lime and fly-ash stabilized steel-slag and crushed-stone pavement base materials. *J. Hunan Univ.* **2012**, *39*, 1–6.
72. Rajakumaran, K. An experimental analysis on stabilization of expansive soil with steel slag and fly ash. *Int. J. Adv. Eng. Technol.* **2015**, *7*, 1745.
73. Shen, W.; Zhou, M.; Ma, W.; Hu, J.; Cai, Z. Investigation on the application of steel slag–fly ash–phosphogypsum solidified material as road base material. *J. Hazard. Mater.* **2009**, *164*, 99–104. [[CrossRef](#)] [[PubMed](#)]
74. Cao, B. *Application of Lime Fly Ash Steel Slag in Pavement Base*; Chang’an University: Xi’an, China, 2004.
75. Zhang, H.; Yu, M.; Li, X. Pavement Performance of Lime–Fly Ash Slag Mixture. *J. Chongqing Jiaotong Univ.* **2011**, *30*, 1344–1346.
76. Wu, R.; Zhang, L.; Han, Z.; Fan, J. Long-term water immersion and freeze-thaw cycles experiment of cement-stabilized macadam bases. *J. Huazhong Univ. Sci. Technol.* **2011**, *39*.
77. Yu, J. *Research on the Experiments about the Pavement Performance of Cement-Fly Ash Stabilized Steel Slag*; Nanjing Forestry University: Nanjing, China, 2010.
78. Özkan, Ö.; Sarıbiyik, M. Alkali silica reaction of BOF and BFS wastes combination in cement. *J. Civ. Eng. Manag.* **2013**, *19*, 113–120. [[CrossRef](#)]
79. Zhang, T.; Yu, Q.; Wei, J.; Li, J. Investigation on mechanical properties, durability and micro-structural development of steel slag blended cements. *J. Therm. Anal. Calorim.* **2012**, *110*, 633–639. [[CrossRef](#)]
80. Mechtcherine, V.; Gram, A.; Krenzer, K.; Schwabe, J.-H.; Shyshko, S.; Roussel, N. Simulation of fresh concrete flow using Discrete Element Method (DEM): Theory and applications. *Mater. Struct.* **2014**, *47*, 615–630. [[CrossRef](#)]
81. Wang, G.; Chen, X.; Dong, Q.; Yuan, J.; Hong, Q. Mechanical performance study of pervious concrete using steel slag aggregate through laboratory tests and numerical simulation. *J. Cleaner Prod.* **2020**, *262*, 121208. [[CrossRef](#)]
82. Wang, S.; Chen, G.; Zhang, L.; Yuan, J. Triaxial discrete element simulation of soil–rock mixture with different rock particle shapes under rigid and flexible loading modes. *Int. J. Geomech.* **2021**, *21*, 04021142. [[CrossRef](#)]
83. Wu, Y. *The Effect of Freeze-Thaw Cycles on the Performance of Cement Stabilized Steel Slag Base*; Hebei University of Engineering: Handan, China, 2020.

84. Wang, S.; Chen, G.; Zhang, L. Parameter inversion and microscopic damage research on discrete element model of cement-stabilized steel slag based on 3D scanning technology. *J. Hazard. Mater.* **2021**, *424*, 127402. [[CrossRef](#)]
85. Du, Z.; Zhu, X. Molecular Dynamics Simulation to Investigate the Adhesion and Diffusion of Asphalt Binder on Aggregate Surfaces. *Transp. Res. Rec. J. Transp. Res. Board* **2019**, *2673*, 500–512. [[CrossRef](#)]
86. Xu, G.; Wang, H. Molecular dynamics study of oxidative aging effect on asphalt binder properties. *Fuel* **2017**, *188*, 1–10. [[CrossRef](#)]
87. Xu, G.; Wang, H. Study of cohesion and adhesion properties of asphalt concrete with molecular dynamics simulation. *Comput. Mater. Sci* **2016**, *112*, 161–169. [[CrossRef](#)]
88. Huang, M.; Zhang, H.; Gao, Y.; Wang, L. Study of diffusion characteristics of asphalt–aggregate interface with molecular dynamics simulation. *Int. J. Pavement Eng.* **2021**, *22*, 319–330. [[CrossRef](#)]
89. Horvath, A. *Life-Cycle Environmental and Economic Assessment of Using Recycled Materials for Asphalt Pavements*; University of California Transportation Center: Berkeley, CA, USA, 2003.
90. Anastasiou, E.; Liapis, A.; Papagianni-Papadopoulou, I.; Memet, M. *Comparative Life Cycle Assessment of Concrete Road Pavements*; Aristotle University of Thessaloniki: Saronica, Greece, 2013.
91. Li, D.; Wang, Y.; Liu, Y.; Sun, S.; Gao, Y. Estimating life-cycle CO₂ emissions of urban road corridor construction: A case study in Xi'an, China. *J. Clean. Prod.* **2020**, *255*, 120033. [[CrossRef](#)]
92. Li, H.; Feng, Z.; Ahmed, A.T.; Yombah, M.; Cui, C.; Zhao, G.; Guo, P.; Sheng, Y. Repurposing waste oils into cleaner aged asphalt pavement materials: A critical review. *J. Clean. Prod.* **2022**, *334*, 130230. [[CrossRef](#)]
93. Pasetto, M.; Pasquini, E.; Giacomello, G.; Baliello, A. Life-Cycle Assessment of road pavements containing marginal materials: Comparative analysis based on a real case study. In *Pavement Life-Cycle Assessment*; CRC Press: Boca Raton, FL, USA, 2017; pp. 199–208.
94. Lee, K.-M.; Park, P.-J. Estimation of the environmental credit for the recycling of granulated blast furnace slag based on LCA. *Resour. Conserv. Recycl.* **2005**, *44*, 139–151. [[CrossRef](#)]
95. Saade, M.R.M.; da Silva, M.G.; Gomes, V. Appropriateness of environmental impact distribution methods to model blast furnace slag recycling in cement making. *Resour. Conserv. Recycl.* **2015**, *99*, 40–47. [[CrossRef](#)]
96. Kang, L.; Du, H.; Zhang, H.; Ma, W. Systematic research on the application of steel slag resources under the background of big data. *Complexity* **2018**, *2018*, 6703908. [[CrossRef](#)]
97. Anastasiou, E.; Liapis, A.; Papayianni, I. Comparative life cycle assessment of concrete road pavements using industrial by-products as alternative materials. *Resour. Conserv. Recycl.* **2015**, *101*, 1–8. [[CrossRef](#)]
98. O'Brien, K.R.; Ménaché, J.; O'Moore, L.M. Impact of fly ash content and fly ash transportation distance on embodied greenhouse gas emissions and water consumption in concrete. *Int. J. Life Cycle Assess.* **2009**, *14*, 621–629. [[CrossRef](#)]
99. *JTG E60-2008*; Code for Field Test of Highway Subgrade and Pavement. Ministry of Transport of the People's Republic of China: Beijing, China, 2008.